

Research Article

Optimization of Cold Spray Process Inputs to Minimize Porosity and Maximize Hardness of Metal Matrix Composite Coatings on AZ31B Magnesium Alloy

Ashokkumar Mohankumar ¹, Thirumalaikumarasamy Duraisamy,¹
Deepak Sampathkumar,² Sathiyamoorthy Ranganathan,³ Guruprasad Balachandran,⁴
Murugan Kaliyamoorthy,⁵ Mathanbabu Mariappan,⁶ and Lijalem Mulugeta ⁷

¹Department of Manufacturing Engineering, Annamalai University, Annamalai Nagar, 608002 Tamil Nadu, India

²Department of Mechanical and Automation Engineering, Agni College of Technology, Thalambur, Chennai-600130, Tamilnadu, India

³Department of Mechanical Engineering, Institute of Road Transport Polytechnic College, Krishnagiri-635104, India

⁴Department of Mechanical Engineering, Alagappa Chettiar Government College of Engineering and Technology, Karaikudi, 630003 Tamil Nadu, India

⁵Department of Mechanical Engineering, Government Polytechnic College, Valangaiman, Thiruvavur, 612804 Tamil Nadu, India

⁶Department of Mechanical Engineering, Government College of Engineering, Bargur, Krishnagiri-635104, India

⁷Department of Mechanical Engineering, Faculty of Manufacturing Institute of Technology, Hawassa University, Ethiopia

Correspondence should be addressed to Lijalem Mulugeta; lijalem@hu.edu.et

Received 1 February 2022; Revised 7 March 2022; Accepted 30 March 2022; Published 30 April 2022

Academic Editor: V. Vijayan

Copyright © 2022 Ashokkumar Mohankumar et al. This is an open access article distributed under the Creative Commons Attribution License, which permits unrestricted use, distribution, and reproduction in any medium, provided the original work is properly cited.

In this investigation, the development of an empirical relationship to determine the porosity and microhardness of the coatings through low-pressure cold-sprayed (LPCS) aluminum alloy/alumina metal matrix composite (MMC) deposit. Spray parameters like temperature, standoff distance (SOD), and powder feed rate play an essential part in the determination of the coating effectiveness. In this study, 3 variables, 5 levels of central composite rotatable design (CCD) were used to decrease the total count of the experimentation. A mathematical model has been developed to evaluate the porosity and hardness of the coated samples along with LPCS spray parameters, and the model's applicability was inspected by ANOVA. Utilizing response surface methodology, spray parameter optimization was carried out. The deposit developed by optimal spray parameters produces the lowest surface porosity of 3.31 vol.% and a higher hardness of 137.21 HV compared with other coated samples. It is validated through the response graph. As a result, the optimized parameters for aluminum alloy/alumina metal matrix composite (MMC) coatings via LPCS are 500 degrees Celsius, 10 mm SOD, and 20 grams/min powder feed rate.

1. Introduction

Magnesium (Mg) and its alloys have received increased attention in a broad range of automobile and aerospace applications due to their high strength-to-weight ratio, higher stiffness, and lower density. Although in some applications, Mg alloys have excellent surface characteristics;

their tribological and electrochemical behavior is poor. Numerous coating processes, such as high velocity oxy fuel (HVOF) and atmospheric plasma spray (APS), can be used to enhance the surface characteristics of Mg alloys. However, the above processes are limited by their performance due to high amount of energy required to fabricate the coatings [1].

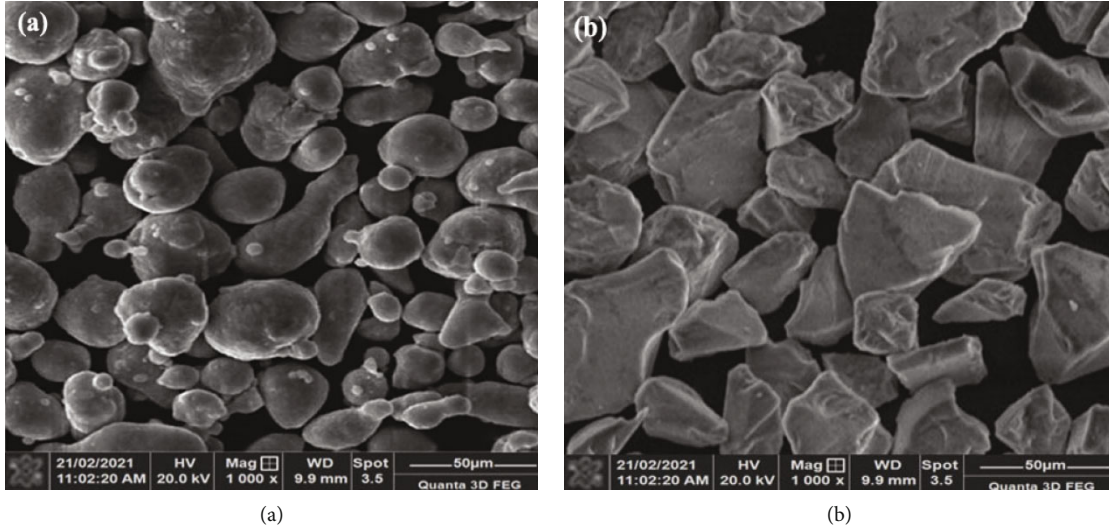
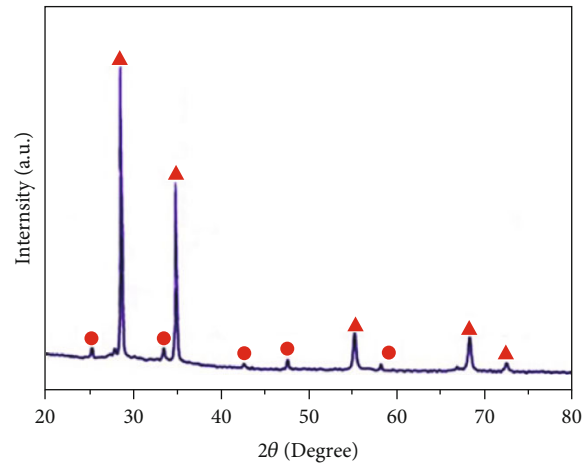
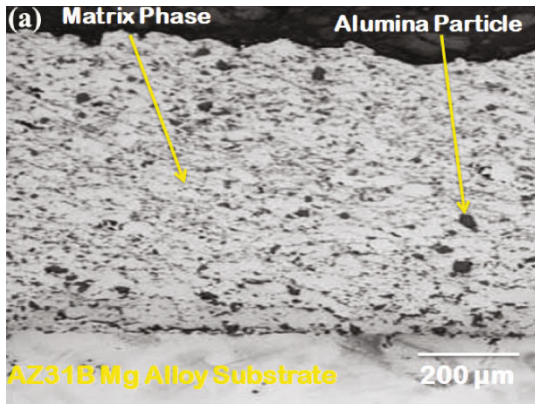


FIGURE 1: SEM morphology of coating material: (a) Al alloy powder; (b) alumina powder.

TABLE 1: LPCS spray parameters and their ranges.

S. no	Parameter	Notation	Ranges				
			-1.682	-1	0	+1	1.682
1	Temperature (degree)	T	450	470.27	500	529.73	550
2	Standoff distance (mm)	D	5	7.02	10	12.97	15
3	Powder feed rate (g/min)	P	15	17.02	20	22.97	25



(a)

(b)

FIGURE 2: (a) Cross-sectional optical microstructural view. (b) XRD of the LPCS MMC coatings.

Low-pressure cold spray (LPCS) is a solid form of depositing process that accelerates the coating material with a high impact on a substratum to produce a deposit. In the cold spray (CS), the coating powder is fed into a convergent-divergent nozzle to generate a supersonic flow. When the

coating powder reaches above the critical velocity, the coating material is deposited on the substratum owing to extreme plastic deformation of the impacting powder materials. In this technique, the temperature of the coating material should be kept below the melting temperature [2–5]. It

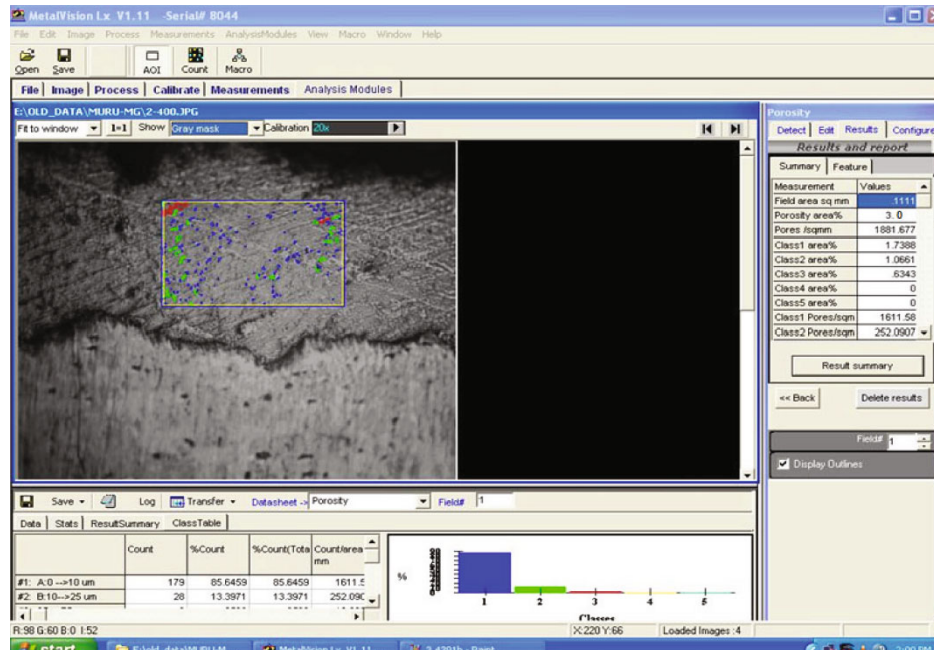


FIGURE 3: Porosity measurement through image analysing software.

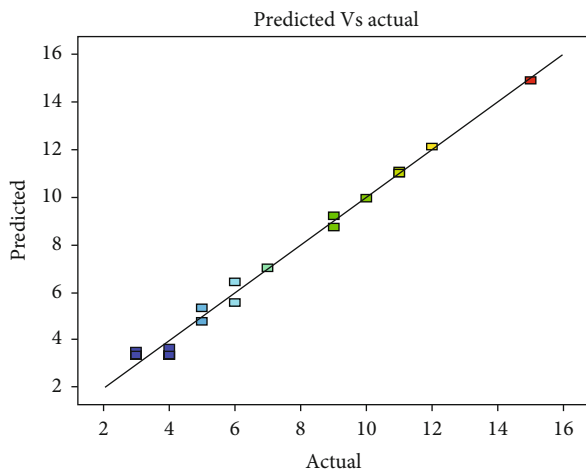


FIGURE 4: Correlation graph (porosity).

has been widely employed in the production of a wide range of metallic deposits like Cu, Al, Ni, and Ti [6, 7].

In order to enhance the properties of the metallic deposit, reinforced ceramic particles were added into the metallic powder to generate the MMC deposit. Aluminum oxide/alumina/ Al_2O_3 is the most popular reinforced ceramic powder for the CS process [8–10]. The wear and porosity behavior of the bronze/alumina MMC coatings is fabricated through atmospheric plasma spray and the CS process. The findings revealed that increasing the alumina concentration in MMC coatings manufactured using plasma and CS processes improved the tribological properties of the coatings, with CS coatings significantly outperforming plasma spraying [11]. The same results have been obtained for copper-

alumina-based MMC deposits with varying sizes and alumina volume percentages. According to the findings, the tribological characteristics of all MMC deposits, including varied volume fractions and sizes of alumina powder, were less compared with the Cu coating. The wear resistance is highly improved when the reinforcement particles have a smaller size of 2–12 microns compared with a larger particle size of 15–45 microns [12]. Other studies on aluminum/alumina, 6061-aluminum/alumina coated on AZ91E Mg alloy substratum by the LPCS process have been reported [10]. They discovered decrease in wear rate when comparing MMC deposits to solid aluminum with 12 weight percent silicon, 356.0 aluminum, and AZ91E T6. Few research studies have shown that mixing alumina particles with metallic powder in CSed composite deposits results in superior hardness compared with raw metallic deposits.

Qui et al. investigated the cold-sprayed A380 Al alloy, discovering that due to their higher strength, the A380 splats deformed remarkably little by the LPCS process. As a result, the surface porosity of the deposit was considerably high [12]. They revealed that the presence of ceramic elements in metallic powder creates a peening impact in cold spray, which has a direct impact on coating characteristics and deposit effectiveness [13, 14]. As a theory, the presence of alumina particles in the metal powder will improve the degree of deformation of A380 metal elements, resulting in less porosity in the coated sample. This will improve the hardness of the coatings, resulting in higher wear resistance [15]. From this is the recalibration or repair of a variety of aluminum and magnesium alloy parts [16]. Nevertheless, magnesium has a hexagonal, close-packed crystalline structure, so any type of magnesium alloy particle does not take deformation sufficiently to form dense coatings. As a result,

TABLE 2: DOE and outcomes.

Exp. condition	Actual values			Outcomes	
	Temperature (°C)	Standoff distance (mm)	Powder feed rate (g/min)	Porosity (vol.%)	Hardness (HV)
1	470.27	7.02	17.02	9	93
2	529.73	7.02	17.02	5	128
3	470.27	12.97	17.02	11	88
4	529.73	12.97	17.02	4	129
5	470.27	7.02	22.97	7	109
6	529.73	7.02	22.97	6	122
7	470.27	12.97	22.97	15	83
8	529.73	12.97	22.97	10	99
9	450	10	20	11	91
10	550	10	20	3	132
11	500	5	20	6	120
12	500	15	20	12	98
13	500	10	15	5	115
14	500	10	25	9	101
15	500	10	20	3	140
16	500	10	20	4	135
17	500	10	20	3	138
18	500	10	20	4	134
19	500	10	20	3	137
20	500	10	20	3	139

repair or reprocessing of defected AZ31 Mg alloys with the same coating material becomes a difficult task as a result of poor wear resistance in the movable components. The coating characteristics of this LPCS MMC coating (including low-weight aluminum alloy with alumina powder) are significantly improved [17]. Hence, it is necessary to improve the Mg alloy product in order to extend its serviceability for industrial applications.

According to the literature review, no study was conducted on the LPCS technique for coating the MMC coating (aluminum alloy/alumina) on AZ31B magnesium alloy. From this, an attempt was made to acquire the best process parameters for MMC deposits to attain higher hardness and low porosity in the coatings. Then, response surface methodology (RSM) was used to optimize the hardness and porosity of the coatings.

2. Experimentation

The LPCS system (mode: Dymet 423, Russia) was employed for this experiment to fabricate the MMC coatings (Al alloy (4.6 wt.% of Cu and 1.4% Mg and Mn of 0.2 wt.)/alumina). The coating materials are as shown in Figures 1(a) and 1(b). Al alloy powder has a size of 6–58 μm and alumina has a size of 20–45 μm . Coating powder was blended with a weight percentage of 80 wt.% of Al alloy and 20 wt.% of alumina using ball milling (VB ceramics, Chennai, India). Before coating, grit blasting was done on the base material surface using corundum grits with a size of $500 \pm 350 \mu\text{m}$ to enhance

the adhesive behavior between the deposit and the base material. The substratum was washed using propanone. The coating was produced on the 5 mm thick AZ31B magnesium alloy substrate. During the coating process, the air pressure of 10 bar is kept constant, and other spray parameters are illustrated in Table 1.

2.1. Coating Characterization. Figure 2 illustrates the XRD and cross-sectional microstructure (optical microscope) (Mitutoyo, Japan; model: AE120) view of the LPCSed Al alloy/alumina coating through optimized spray parameters. From this figure, the interfacial bonding between the deposit and the base material is free of porosity, and good adhesion takes place between the base materials. The cold spray process has a feature that allows for excellent adherence and density deposit, which aids in the production of high-density coatings [12]. The alumina seems to be well retained in the deposit; nevertheless, the alumina phase appears to be dispersed unevenly. This results in the varied hardness in various regions of the deposit; the hardness was measured in 10 various regions of the coating. As a result, the optimized spray parameter hardness of the deposit is about 140 HV_{0.03} measured by the Vickers microhardness tester (Mitutoyo; model: HM-200 system D). Several authors have discovered the same microstructure characteristics for cold-sprayed deposits [8, 10, 13].

As shown in Figure 3, the porosity of the optimized parameters of the coatings for the surface was about 3%, measured using an optical microscope with image analysis

TABLE 3: Porosity and hardness images for experimental condition.

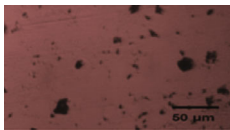
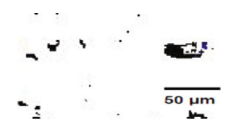
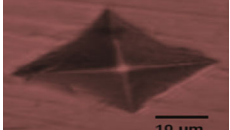
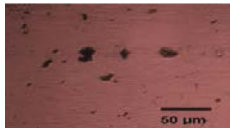

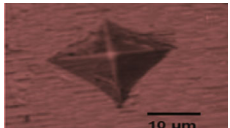
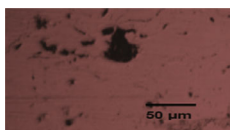
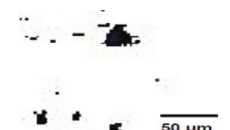
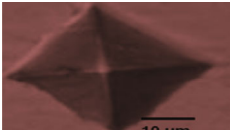
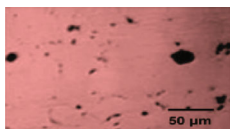

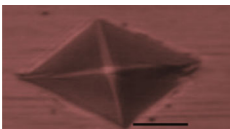



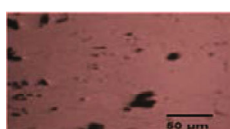

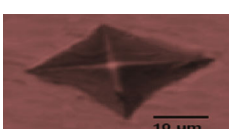
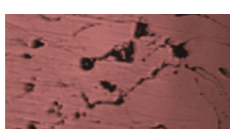

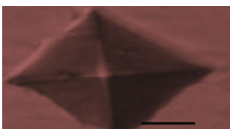


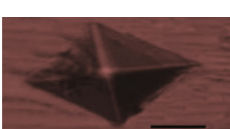

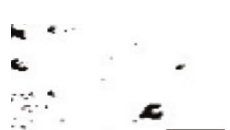




No. of experiments	Microstructure of porosity analysis	Binary images of the porosity analysis	Hardness indentation
Exp. no: 01 <i>T</i> : 470.27 <i>D</i> : 7.02 <i>P</i> : 17.02			
Exp. no: 02 <i>T</i> : 529.73 <i>D</i> : 7.02 <i>P</i> : 17.02			
Exp. no: 03 <i>T</i> : 470.27 <i>D</i> : 12.97 <i>P</i> : 17.02			
Exp. no: 04 <i>T</i> : 529.73 <i>D</i> : 12.97 <i>P</i> : 17.02			
Exp. no: 05 <i>T</i> : 470.27 <i>D</i> : 7.02 <i>P</i> : 22.97			
Exp. no: 06 <i>T</i> : 529.73 <i>D</i> : 7.02 <i>P</i> : 22.97			
Exp. no: 07 <i>T</i> : 470.27 <i>D</i> : 12.97 <i>P</i> : 22.97			
Exp. no: 08 <i>T</i> : 529.73 <i>D</i> : 12.97 <i>P</i> : 22.97			
Exp. no: 09 <i>T</i> : 450 <i>D</i> : 10 <i>P</i> : 20550			
Exp. no: 10 <i>T</i> : 550 <i>D</i> : 10 <i>P</i> : 20			

TABLE 3: Continued.

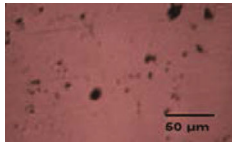
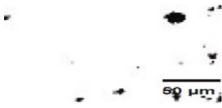
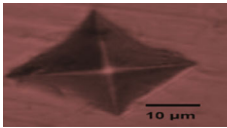
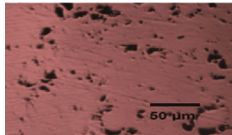
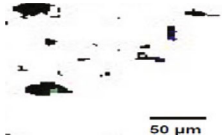
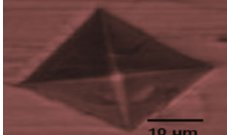
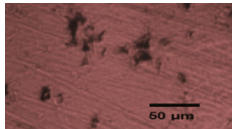
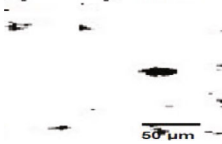
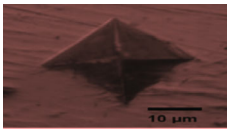
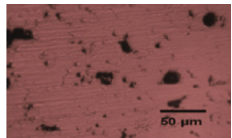
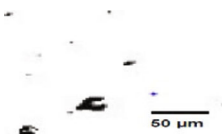
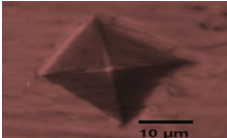
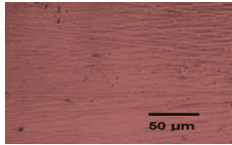
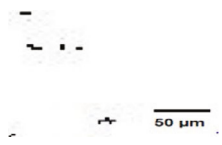
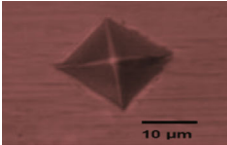
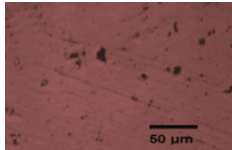
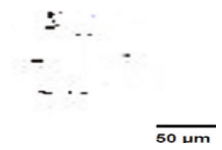
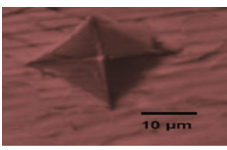
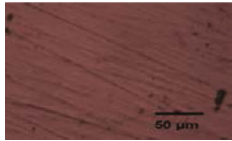
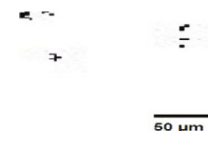
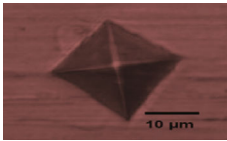
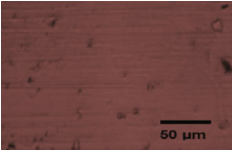
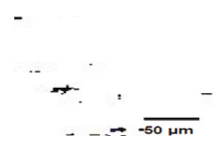
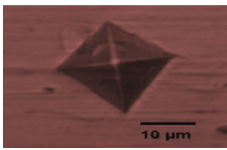
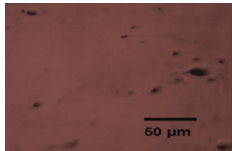

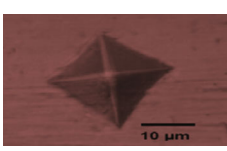
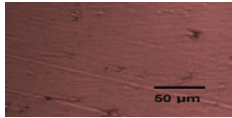
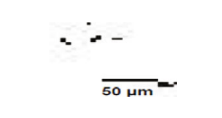
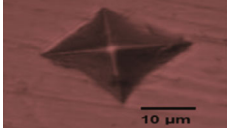
No. of experiments	Microstructure of porosity analysis	Binary images of the porosity analysis	Hardness indentation
Exp. no: 11 <i>T</i> : 500 <i>D</i> : 5 <i>P</i> : 20			
Exp. no: 12 <i>T</i> : 500 <i>D</i> : 15 <i>P</i> : 20			
Exp. no: 13 <i>T</i> : 500 <i>D</i> : 10 <i>P</i> : 15			
Exp. no: 14 <i>T</i> : 500 <i>D</i> : 10 <i>F</i> : 25			
Exp. no: 15 <i>T</i> : 500 <i>D</i> : 10 <i>P</i> : 20			
Exp. no: 16 <i>T</i> : 500 <i>D</i> : 10 <i>P</i> : 20			
Exp. no: 17 <i>T</i> : 500 <i>D</i> : 10 <i>P</i> : 20			
Exp. no: 18 <i>T</i> : 500 <i>S</i> : 10 <i>P</i> : 20			
Exp. no: 19 <i>T</i> : 500 <i>D</i> : 10 <i>P</i> : 20			
Exp. no: 20 <i>T</i> : 500 <i>D</i> : 10 <i>P</i> : 20			

TABLE 4: ANOVA result for porosity.

Source	Sum of squares	Df	Mean square	F value	p value prob > F	
Model	250.15	9	27.79	115.71	<0.0001	Significant
T (temperature)	67.91	1	67.91	282.71	<0.0001	
D (standoff distance)	39.04	1	39.04	162.53	<0.0001	
P (powder feed rate)	18.11	1	18.11	75.40	<0.0001	
TD	6.13	1	6.13	25.50	0.0005	
TP	3.13	1	3.13	13.01	0.0048	
DP	15.13	1	15.13	62.96	<0.0001	
T ²	27.86	1	27.86	115.97	<0.0001	
D ²	63.40	1	63.40	263.93	<0.0001	
P ²	27.86	1	27.86	115.97	<0.0001	
Residual	2.40	10	0.2402			
Lack of fit	1.07	5	0.2138	0.8016	0.5929	Not significant
Pure error	1.33	5	0.2667			
Cor. total	252.55	19				

TABLE 5: ANOVA result for hardness.

Source	Sum of squares	Df	Mean square	F value	p value prob > F	
Model	7203.82	9	800.42	194.60	<0.0001	Significant
T (temperature)	2215.72	1	2215.72	538.68	<0.0001	
D (standoff distance)	593.10	1	593.10	144.19	<0.0001	
P (powder feed rate)	172.56	1	172.56	41.95	<0.0001	
TD	10.13	1	10.13	2.46	0.1477	
TP	276.12	1	276.12	67.13	<0.0001	
DP	253.13	1	253.13	61.54	<0.0001	
T ²	1267.92	1	1267.92	308.25	<0.0001	
D ²	1518.14	1	1518.14	369.09	<0.0001	
P ²	1624.53	1	1624.53	394.95	<0.0001	
Residual	41.13	10	4.11			
Lack of fit	14.30	5	2.86	0.5329	0.7468	Not significant
Pure error	26.83	5	5.37			
Cor. total	7244.95	19				

software based on ASTM B 276. At the time of the coating process, when the coating material feed rate increases, the harder elements (alumina) rebound from the coated surface, which causes the deposit flaws that lead to the coating porosity.

In this investigation, alumina blending of 20 wt.% with Al alloy powder was kept constant because increasing the hard element percentage in the coating will decrease the deposition efficiency owing to the hard particle rebound while spraying against the substrate, as acknowledged by Spencer et al. [10].

2.2. Identification of Process Parameters. The initial step in the design of the experiment is to select the spray parameters that will be explored. In general, all parameters impact on the characteristics of the deposit. The prominent parameters

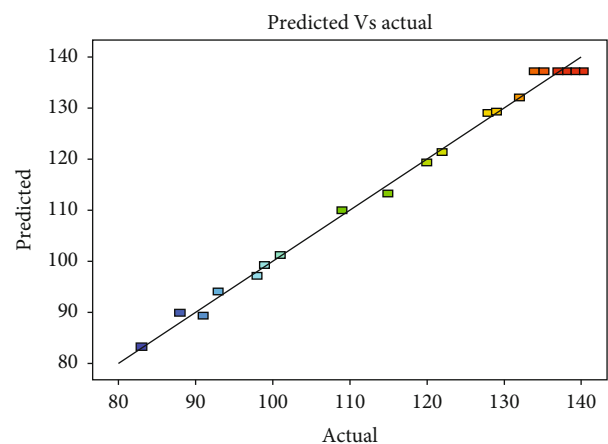


FIGURE 5: Correlation graph (hardness).

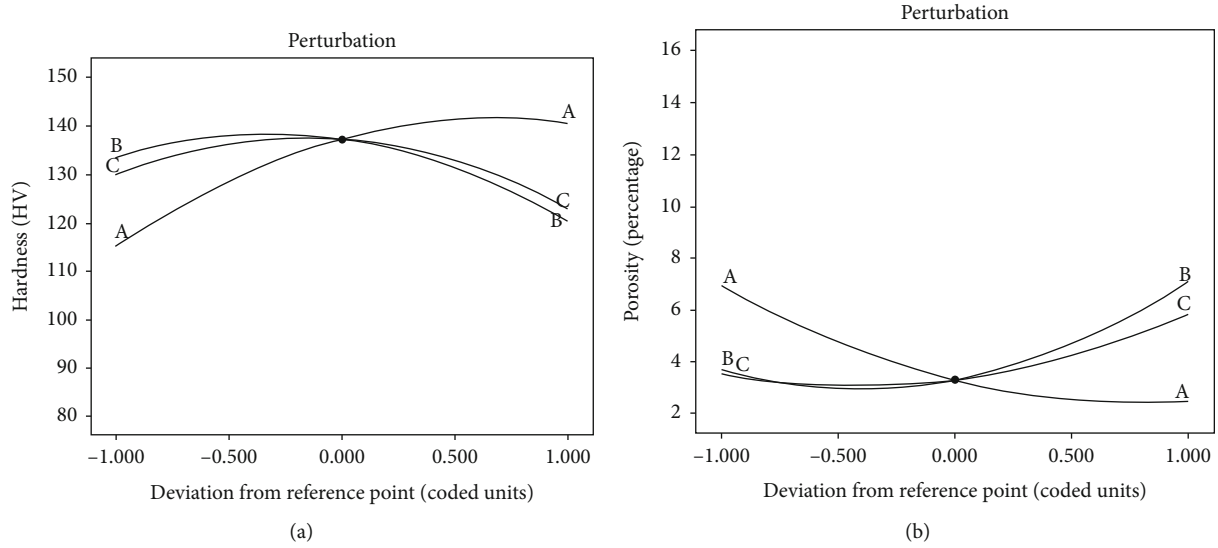


FIGURE 6: Perturbation plots: (a) hardness; (b) porosity.

that had a higher impact on the deposit were chosen based on previously published work [18, 19]. The selected factors are temperature, SOD, and powder feed rate. A higher number of experimental tests were conducted to identify the possible operating ranges for LPCS.

2.3. Identifying the Parameter's Operational Limits. To determine the feasible operational range of the aforesaid parameters, a vast number of tests are carried out on the AZ31B Mg alloy substratum by changing one of the LPCS process variables and maintaining the other parameters intact. Numerous tests were carried out by varying the variables of the LPCS, and the findings during coating are depicted in Figure 4.

If the temperature was below 500°C, the coating powder heating and softening do not take place, and the adhesive properties between the substrate and the coating are very poor. If the temperature is above 550°C, the melting of coating powder affects the coating principle of CS. Nozzle blocking occurs because of melting. The maximum possible temperature is 600°C (restriction in the temperature supply of the Dymet 423 LPCS process).

If the SOD was below 5 mm, the coating material does not stick to the substrate; it bounces back, so the deposition rate is very low. Above 15 mm, the spray plume becomes unstable and not able to reach the substrate. Deposition does not take place.

If the feed rate of the coating material is below 15 g/min, uniform deposition does not take place because the flow of coating powder is less. Above 25 g/min, the coating thickness increases dramatically, and the cohesive properties of the deposit are very poor.

2.4. Development of DOE Matrix. Depending on the conditions listed in the previous section, the feasible working range of the LPCS process parameters was determined by the spraying being completed without substratum faults

and the coated sample exhibiting excellent adherence and cohesion behavior. RSM is employed to determine the relationship between the major input parameters and output responses (porosity and hardness). DOE and optimization were conducted through "Design Expert Software 11" with 3 variables, and a 5-level CCD matrix was selected. Table 2 shows the coating factor levels. Table 3 shows the total 20 experiment parameters and their responses by means of microstructural, binary images of porosity and hardness indentation images of the coated sample. Then, the high and low range of the variables was +1.682 and -1.682. Equation (1) is used to determine the coded values of any intermediate value.

$$Y_i = 1.682 [2Y - (Y_{\text{maximum}} + Y_{\text{minimum}}) / (Y_{\text{maximum}} + Y_{\text{minimum}})], \quad (1)$$

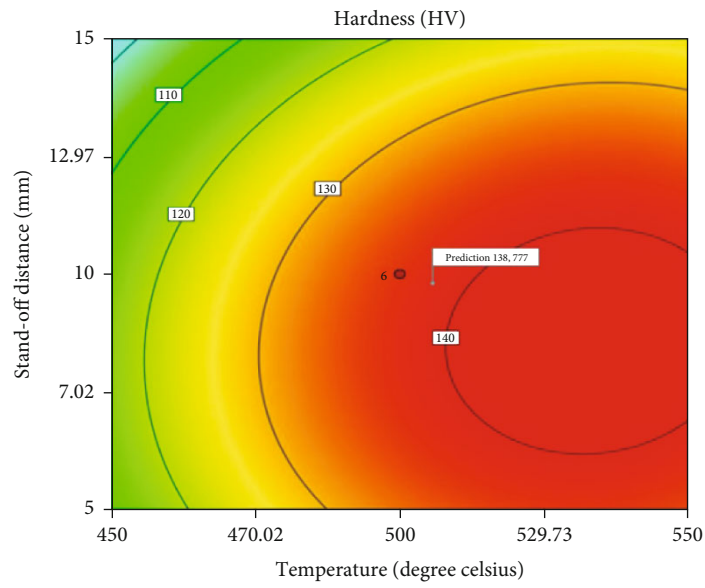
where Y_i is the coded value essential for the Y variable, Y represents any variable value between Y_{minimum} and Y_{maximum} , and the smaller range and higher range of the variables were indicated through Y_{minimum} and Y_{maximum} .

2.5. Development of Empirical Relationships. In the current study, in order to relate the coating parameters to the outcomes of LPCS coatings, a 2nd order polynomial function was constructed to determine the outcome of the experimentally obtained values. It is illustrated below.

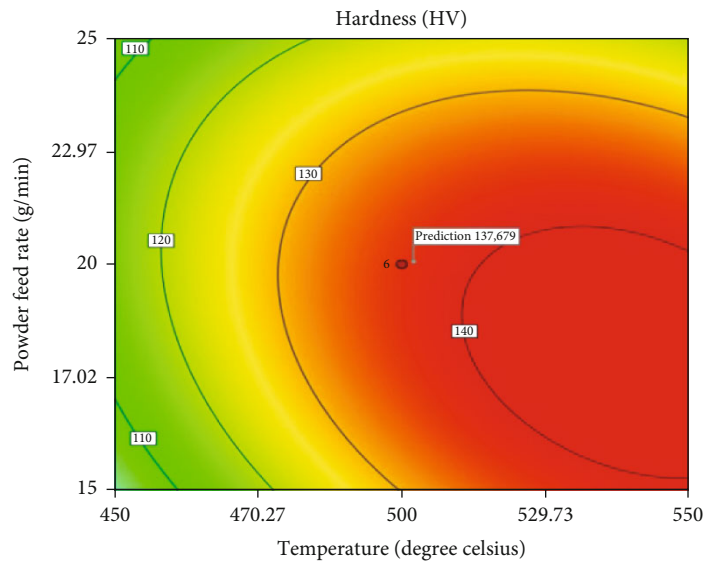
$$Z = a_0 + \sum a_i x_i + \sum a_{ii} x_i^2 + \sum a_{ij} x_i x_j. \quad (2)$$

The outcome (porosity and microhardness) is a function of temperature (T), standoff distance (D), and powder feed rate (P), and it can be indicated as

$$\text{Responses} = f(T, D, P). \quad (3)$$

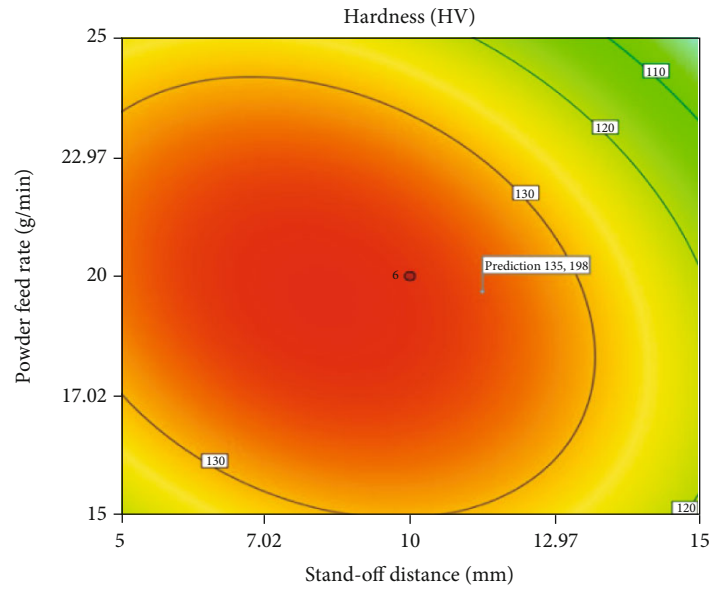


(a)

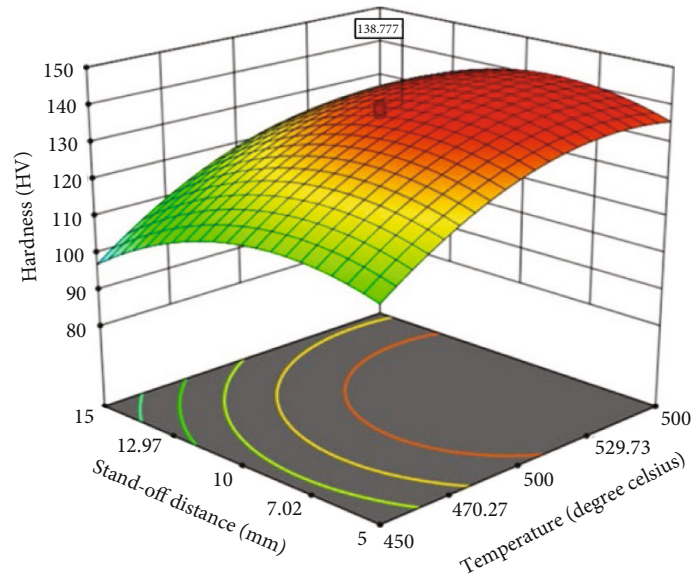


(b)

FIGURE 7: Continued.

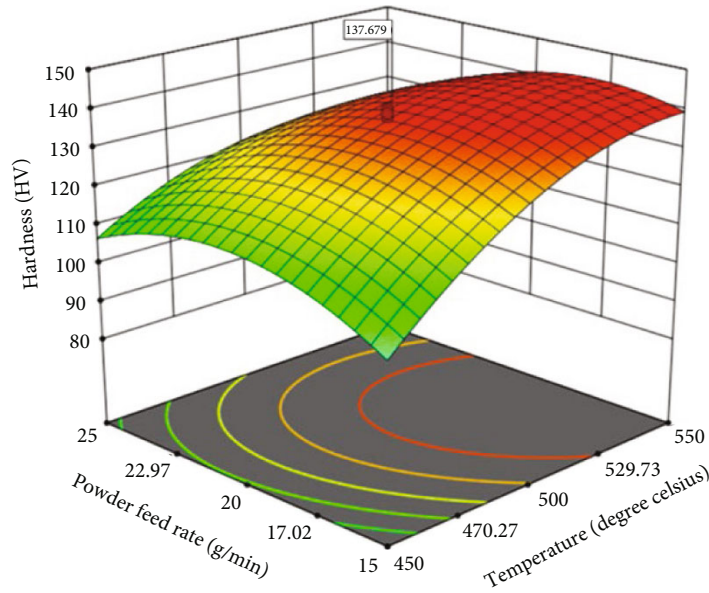


(c)

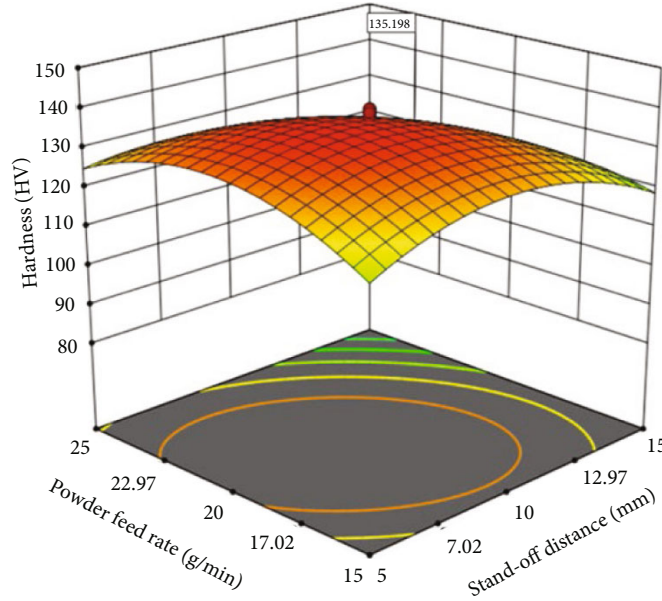


(d)

FIGURE 7: Continued.



(e)



(f)

FIGURE 7: (a–c) Contour graph and (d–f) response graph for hardness.

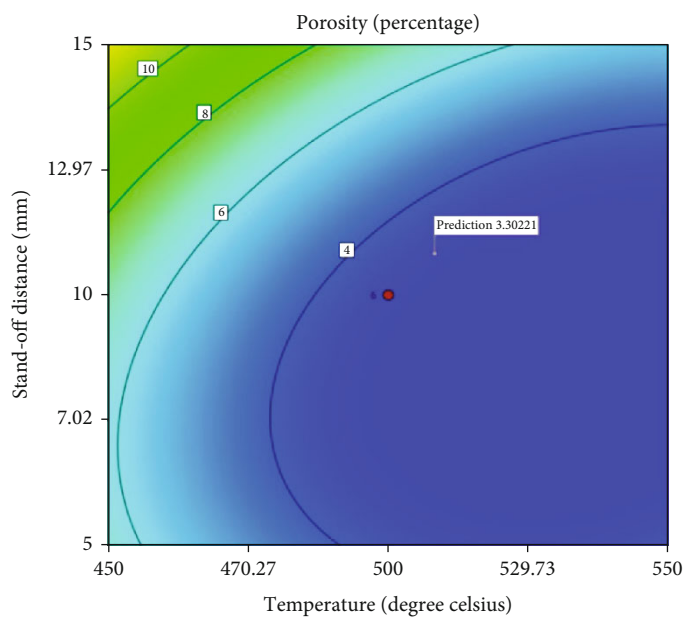
For three factors, the chosen polynomial was indicated as

$$Z = a_0 + a_1(T) + a_2(D) + a_3(P) + a_{11}(T^2) + a_{22}(D^2) + a_{33}(P^2) + a_{12}(TD) + a_{13}(TP) + a_{23}(DP), \quad (4)$$

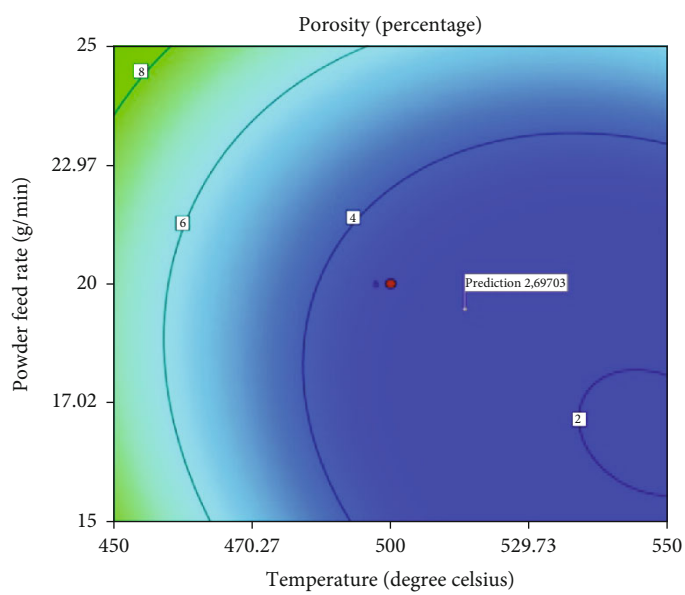
where a_0 is the average response value; the coefficients a_1, a_2, \dots, a_{23} are based on the linear, interactive, and square terms of factors. In this study, design expert software was utilized to compute the coefficients. The Student t -test and p values were adopted to know about the needs

of each coefficient and are illustrated in Tables 4 and 5. The following empirical relations were generated through these coefficients, which include important factors on their own.

$$\begin{aligned} \text{Porosity (volume\%)} = & 3.32 - 2.23(T) + 1.69(D) \\ & + 1.15(P) - 0.87(TD) + 0.62(TP) \\ & + 1.38(DP) + 1.39(T)^2 + 2.10(D)^2 \\ & + 1.39(C)^2, \end{aligned} \quad (5)$$



(a)



(b)

FIGURE 8: Continued.

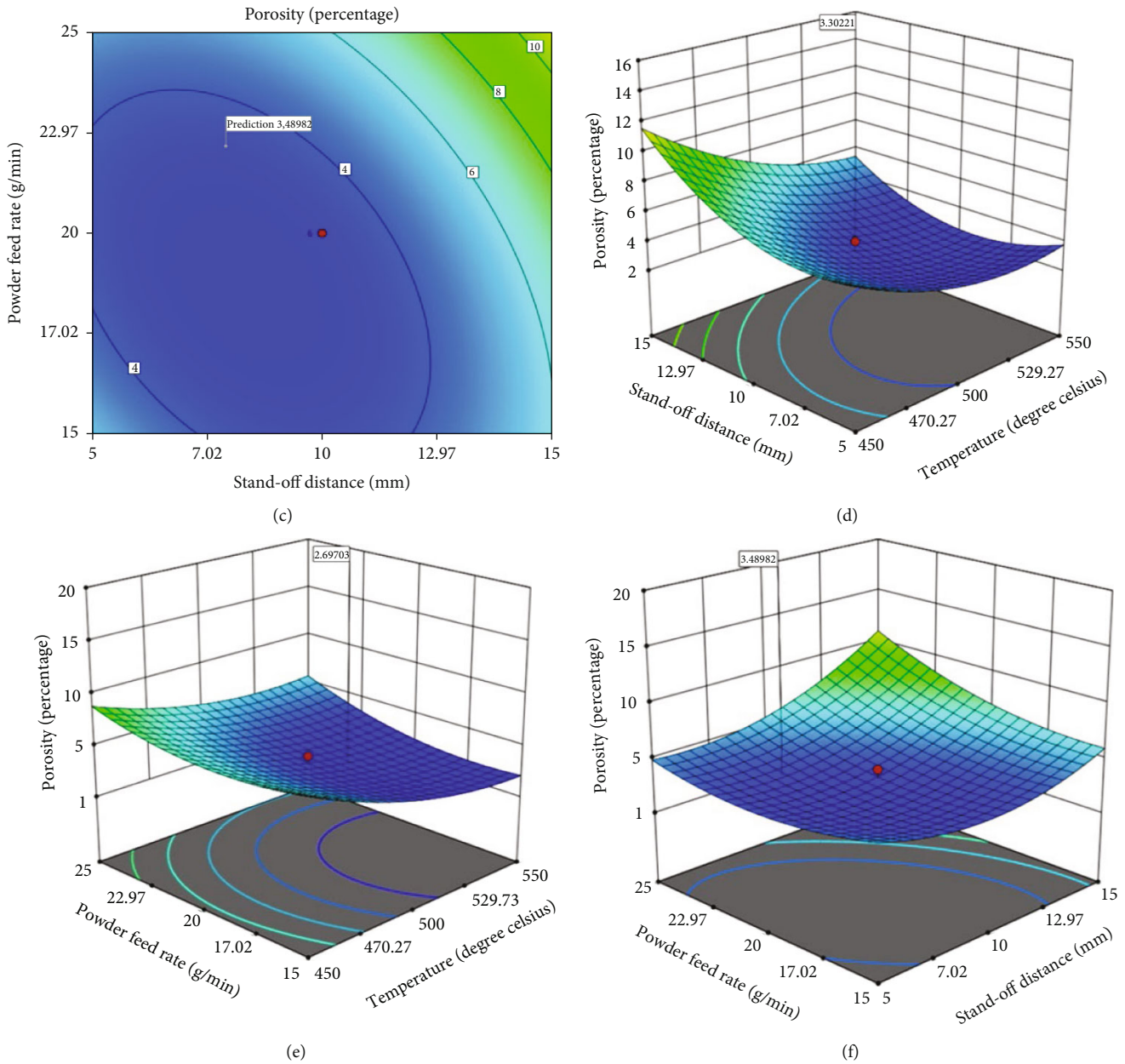


FIGURE 8: (a-c) Contour graph and (d-f) response graph for porosity.

$$\begin{aligned}
 \text{Hardness (HV}_{0.03}) &= 137.21 + 12.74 (T) + 6.59 (D) \\
 &\quad - 3.55 (P) + 1.13 (TD) - 5.87 (TP) \\
 &\quad - 5.62 (DP) - 9.38 (T)^2 - 10.26 (D)^2 \\
 &\quad - 10.26 (P)^2.
 \end{aligned}
 \tag{6}$$

The probability greater than F less than 0.05 denotes that the model is highly significant. R^2 values were determined to be 0.9951 and 0.9946, respectively. This means that 99.51% and 99.46% of the experimental outcomes accord with the proof anticipated through the known observational relationship. R^2 ranging between 0 and 1

indicates that the empirical relation developed is appropriate. The R^2 value must be near to 1.0, indicating that the statistical model generated is more accurate. The figure suggests that the residual fall of the straight line represents the flaws. The distribution of the flaws is normal. Figures 4 and 5 illustrate that the value obtained closely correlates with the experimental results.

3. Results and Discussion

In this investigation, a numerically and graphically optimized approach was used to determine the porosity and hardness of the LPCS deposit. Because the inverse correlation between porosity and hardness was well established in

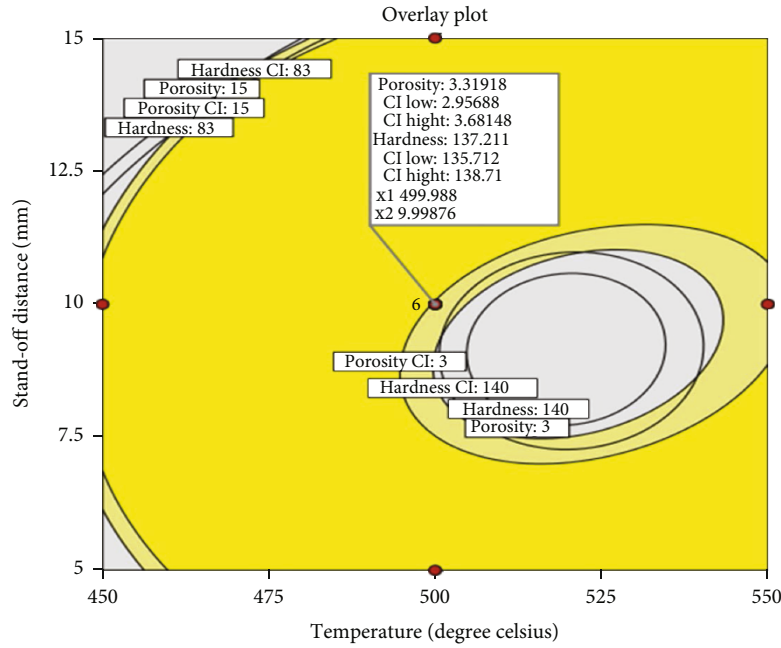


FIGURE 9: Overlay plot.

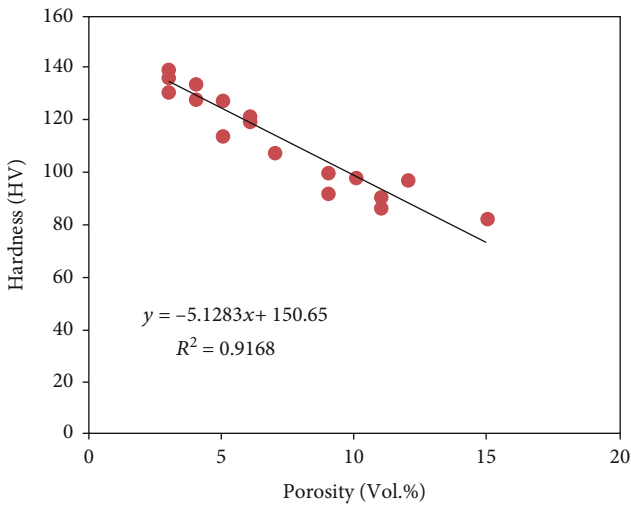


FIGURE 10: Relationship between porosity and hardness.

the LPCS deposit, the choice was made to improve hardness and reduce porosity. The best condition was obtained by setting constraints on output responses and on the process parameters. As indicated in Figure 6, the level of porosity of the deposit was predicted and exhibited based on the obtained regression equation.

As illustrated in Figure 7, the powder feed rate is the most important coating parameter because it reveals the greatest variation in coating properties. According to Figure 7 and Table 2, it is noticed that the hardness of the deposit raises remarkably when the powder feed rate is increased to the level of 20 g/min. At 20 g/min of powder feed rate, the alumina particles in the deposit also rise as large amounts of elements are distributed in the LPCS

plume. The presence of ceramic elements in the deposit gives better load distribution ability between the matrix phase and the ceramic elements, resulting in improved hardness. The presence of ceramic particles in the deposit raises the interface region accessible to distribute the load from the matrix phase when loads are applied. Finally, a higher concentration of ceramic elements reduces the mean free route among the ceramic elements, which prevents plastical distortion of the deposit in load state by preventing void nucleation, resulting in improved deposit hardness.

The coating properties show better results with the optimized standoff distance of 10 mm as shown in Figure 7. Therefore, by raising the standoff distance above 10 mm, the properties of coatings go down. The variance in coating properties as the standoff distance increases is based on the impact velocity of the coating material. At 10 mm of SOD, the powder elements' impact in flight velocity is raised; thus, the impact velocity of the elements is very high. Therefore, very high impacting velocity causes a peening reaction in the deposit, which causes it to consolidate and form a very dense coating. It results in the improved hardness of the deposit. Previously, we stated that by raising the standoff distance, the elements' dwell time in the spray plume increases, resulting in higher element temperature. Nevertheless, raising the standoff distance after reaching an optimum level leads to lowering the element temperature as the isothermic in the plume starts to decompose. As a result, raising the standoff distance beyond a particular level causes a reduction in the deposition efficiency and coating hardness. The hardness of the deposit is afflicted by the massive number of reinforcement particles (alumina) in the deposit, despite the fact that the presence of alumina particles in the coating material mixture was kept constant for this investigation. As a result, it is possible to infer that the alumina

TABLE 6: Validation results for optimization.

Exp. no.	Temperature (degree)	Cold spray parameters		Porosity (vol.%)			Microhardness (HV)		
		Standoff distance (mm)	Powder feed rate (g/min)	By experiment	By modal	Variation (%)	By experiment	By modal	Variation (%)
1	510	11	19	4.3	4.5	+3.77	128	134	+4.47
2	513	13	22	5	4.6	-2.56	126	132	+4.54
3	520	12	23	5.3	5	-4.63	135	130	-3.38

TABLE 7: Validation outcomes for developed empirical relationships.

Exp. no.	Temperature (degree)	Cold spray parameters		Coatings	
		Standoff distance (mm)	Powder federate (g/min)	Porosity (vol.%)	Microhardness (HV)
1	560	16	27	7	110
2	440	8	12	13	97
3	460	9	18	11	90

presence in the deposit is maximized when the SOD is 10 mm, resulting in increased hardness as illustrated in Figure 7 and Table 2. The surface hardness of the deposit increases as the temperature rises to 500°C.

Figure 8 illustrates that the porosity of the coating is greatly influenced by powder feed rate and SOD. The deposit's porosity decreases dramatically as the SOD increases to 10 mm. From that, the optimal SOD of 10 mm increases the coating powder dwell span in the plume, resulting in higher particle temperatures. At a temperature of 500°C, the coating powder temperatures promote thermal softening, resulting in flattening the particles that are easy to bind with the early deposited particles. This leads to the pores in the deposits being closed. The porosity of the MMC coatings shows better results at a powder feed rate of 20 g/min, but when the powder feed rate is below 20 and or above 20 g/min, the porosity level in the coatings increases, as presented in Figure 8 and Table 2. Thus, hard particle rebounding will increase with the rising powder feed rate, causing porosity in the rebounded region. Raising the powder feed rate results in a thicker deposit, but the deposit has a higher level of pores owing to particle rebounding, which leads to the porosity level rising in the coating surface.

The multiple-objective optimization concept must be discovered where the criterion fulfills the desirable characteristics simultaneously. As a result, there is a balance between the conditions that must be met by the two techniques. To achieve the objective, the multiple objective optimization method is employed with a specific end aim. The various outcomes were attained through graphical optimization. In the contour graph, the best imposed or highly critical response contours are used to highlight the areas that can meet the stated requirements. It is feasible to visibly verify a good conciliation at this stage. Owing to the handling of many answers, it is recommended that an analytic form of optimization be performed first; otherwise, determining the possible zone could be problematic. Graphical optimization is most

commonly found in the sector of viable areas in the factor zone. The areas shaded are really not suitable for the optimization approach. The next step was to overlap the indicated regions of every outcome to create an intriguing location or a huge plot. Figure 9 depicts the predicted outcomes of the overlay patterning of outcomes (porosity and hardness). For concepts of better hardness and lower porosity, the light-reduced shadow is still used.

As illustrated in Figure 10, the hardness and porosity of the MMC deposit arising from the experimentation data are connected. The experimentation values are best suited by a single straight line.

The regression equation will be used to depict the straight line.

$$\text{Hardness (HV)} = -5.128x + 150.65 \text{ porosity (vol.\%)}. \quad (7)$$

The slope of the approximated regression model (-5.128) is negative, indicating that hardness values rise as porosity falls. The determination coefficient $R^2 = 92\%$. It could be expressed as a percent of the overall sum of squares that can be defined using the approximation regression models. The determination coefficient R^2 is a fit-goodness estimate of the predicted regression model.

The built regression line (Equation (7)) is frequently utilized for two reasons:

- (i) To calculate the hardness standard in relation to the porosity of the deposit
- (ii) Estimating the specific hardness for a particular degree of porosity for the deposit

The confidence and probabilistic intervals indicate if the regression outcomes shorter spacing provides greater precision (Figure 10). The confident interval is an approximated range among the mean value of Y 's and the X 's. PI is an approximation of the individualized value interval of y for

a specified x value. The developed regression model provides a point to determine the mean hardness value for a specified value of porosity. The differentiation among the confident and probabilistic intervals is due to the reason that the mean value of hardness can be measured more precisely than the individualized hardness value. The higher the probabilistic interval, the greater the uncertainty formed by predicted randomized variable value than that of estimated mean value.

3.1. Validation. It is essential to evaluate the determined relationship developed was correct for prediction of the responses in the formation of empirical relations. The prediction ability of the empirical relation developed was examined by running three more experimentation with coating process parameters.

Tables 6 and 7, demonstrate the experimental and expected findings. The anticipated porosity and hardness values estimated from present relation are similar to the experimentation findings and which is 5% of the deviation.

Depending on the results of the investigation, the proposed optimal parameters are provided in Table 6. Cold spray experiments were prepared and carried out with these variables, and other three sets of trials with higher and lower levels of optimum condition outcomes were also carried out, as shown in Table 7.

From this investigation, deviation from the optimized spray parameters results in a rise in porosity as well as a decrease in hardness. This is due to the higher temperature softening of the coating material, variations in SOD, and the time it takes for the coating plume to reach the substrate.

4. Conclusions

A central composite rotatable design was utilized to investigate the effect of coating parameters on the microhardness and porosity of the LPCS aluminum alloy/alumina metal matrix composite (MMC) deposit. The following results were obtained with the goal of improving the coating parameters to enhance coating hardness and reduce the porosity of the deposit.

Empirical relations were generated from the experimentation results that will be utilized to examine the correlation between the variables of the LPCS method and the quality properties of the deposit, such as the porosity and hardness of the MMC deposit by RSM.

According to ANOVA, graphical and numerical study outcomes, powder feed rate and standoff distance were found to be the most predominant factors affecting the porosity and hardness of the deposits, followed by temperature.

The optimum process parameters were determined to be 20 g/min feed rate, 500°C temperature, and 10 mm SOD. By using the above process parameters, the actual value (experimental) coating microhardness was 140 HV, and the porosity was 3 vol.%. The predicted value (contour, response, and overlay plot) coating microhardness was 137.21 HV and porosity was 3.31 vol.%.

Data Availability

The data used to support the findings of this study are included in the article. Should further data or information be required, these are available from the corresponding author upon request.

Disclosure

The study was performed as a part of the employment at Hawassa University, Ethiopia.

Conflicts of Interest

The authors declare that there are no conflicts of interest regarding the publication of this paper.

Acknowledgments

The authors are grateful to the Department of Science and Technology (DST)-Science and Engineering Research Board (SERB), Government of India, New Delhi, for providing financial support for this study under the Empowerment and Equity Opportunities for Excellence in Science (EMEQ) scheme, R&D project file no. EEQ/2018/000472. The project assistant of DRDO Mr. A. Arunkumar is greatly acknowledged for technical support.

References

- [1] J. E. Gray and B. Luan, "Protective coatings on magnesium and its alloys – a critical review," *Journal of alloys and compounds*, vol. 336, no. 1-2, pp. 88–113, 2002.
- [2] H. Assadi, F. Gartner, T. Stoltenhoff, and H. Kreye, "Bonding mechanism in cold gas spraying," *Acta Materialia*, vol. 51, no. 15, pp. 4379–4394, 2003.
- [3] T. Peat, A. Galloway, A. Toumpis, P. McNutt, and N. Iqbal, "The erosion performance of particle reinforced metal matrix composite coatings produced by co-deposition cold gas dynamic spraying," *Applied Surface Science*, vol. 396, pp. 1623–1634, 2017.
- [4] T. Stoltenhoff, H. Kreye, and H. J. Richter, "An analysis of the cold spray process and its coatings," *Journal of Thermal Spray Technology*, vol. 11, no. 4, pp. 542–550, 2002.
- [5] Y. L. Liang, Z. B. Wang, J. Zhang, J. B. Zhang, and K. Lu, "Enhanced bonding property of cold-sprayed Zn-Al coating on interstitial-free steel substrate with a nanostructured surface layer," *Applied Surface Science*, vol. 385, pp. 341–348, 2016.
- [6] T. Suhonen, T. Varis, S. Dosta, M. Torrell, and J. M. Guilemany, "Residual stress development in cold sprayed Al, Cu and Ti coatings," *Acta Materialia*, vol. 61, no. 17, pp. 6329–6337, 2013.
- [7] H. Koivuluoto, J. Lagerbom, and P. Vuoristo, "Microstructural studies of cold sprayed copper, nickel, and nickel-30% copper coatings," *Journal of Thermal Spray Technology*, vol. 16, no. 4, pp. 488–497, 2007.
- [8] Y. Tao, T. Xiong, C. Sun, H. Jin, H. Du, and T. Li, "Effect of α -Al₂O₃ on the properties of cold sprayed Al/ α -Al₂O₃ composite coatings on AZ91D magnesium alloy," *Applied Surface Science*, vol. 256, no. 1, pp. 261–266, 2009.

- [9] E. Irissou, J.-G. Legoux, B. Arsenault, and C. Moreau, "Investigation of Al-Al₂O₃ cold spray coating formation and properties," *Journal of Thermal Spray Technology*, vol. 16, no. 5-6, pp. 661–668, 2007.
- [10] K. Spencer, D. M. Fabijanac, and M. X. Zhang, "The use of Al-Al₂O₃ cold spray coatings to improve the surface properties of magnesium alloys," *Surface and Coating Technology*, vol. 204, no. 3, pp. 336–344, 2009.
- [11] J. M. Miguel, J. M. Guilemany, and S. Dosta, "Effect of the spraying process on the microstructure and tribological properties of bronze-alumina composite coatings," *Surface and Coating Technology*, vol. 205, no. 7, pp. 2184–2190, 2010.
- [12] K. I. Triantou, D. I. Pantelis, V. Guipont, and M. Jeandin, "Microstructure and tribological behavior of copper and composite copper+alumina cold sprayed coatings for various alumina contents," *Wear*, vol. 336-337, pp. 96–107, 2015.
- [13] H. Koivuluoto, J. Lagerbom, M. Kylmälahti, and P. Vuoristo, "Microstructure and mechanical properties of low-pressure cold-sprayed (LPCS) coatings," *Journal of Thermal Spray Technology*, vol. 17, no. 5-6, pp. 721–727, 2008.
- [14] H. Koivuluoto and P. Vuoristo, "Effect of powder type and composition on structure and mechanical properties of Cu +Al₂O₃ coatings prepared by using low-pressure cold spray process," *Journal of Thermal Spray Technology*, vol. 19, no. 5, pp. 1081–1092, 2010.
- [15] S. B. Dayani, S. K. Shaha, R. Ghelichi, J. F. Wang, and H. Jahed, "The impact of AA7075 cold spray coating on the fatigue life of AZ31B cast alloy," *Surface and Coating Technology*, vol. 337, pp. 150–158, 2018.
- [16] N. H. Tariq, L. Gyansah, J. Q. Wang et al., "Cold spray additive manufacturing: a viable strategy to fabricate thick B₄C/Al composite coatings for neutron shielding applications," *Surface and Coating Technology*, vol. 339, pp. 224–236, 2018.
- [17] M.-Z. Ge, J.-Y. Xiang, Y. Tang et al., "Wear behavior of Mg-3Al-1Zn alloy subjected to laser shock peening," *Surface and Coating Technology*, vol. 337, pp. 501–509, 2018.
- [18] W. Jibrán, J. Hogan, and A. McDonald, "Towards optimization of thickness, hardness, and porosity of low-pressure cold sprayed WC-Ni coatings," *International Journal of Advanced Manufacturing Technology*, vol. 116, no. 7-8, pp. 2149–2160, 2021.
- [19] J. Pattison, S. Celotto, A. Khan, and W. O'neill, "Standoff distance and bow shock phenomena in the cold spray process," *Surface and Coating Technology*, vol. 202, pp. 1443–1454, 2018.